Rare Metal Materials and Engineering
Volume 54, Issue 11, November 2025
Available online at www.rmme.ac.cn

Science Press

Cite this article as: Zhang Jingang, Liu Xinling, Chen Xing, et al. Fracture Behavior of Nickel-Based Single Crystal Superalloy During High-Cycle Fatigue at 850 °C[J]. Rare Metal Materials and Engineering, 2025, 54(11): 2777-2785. DOI: https://doi.org/10.12442/j.issn.1002-185X.20240631.

ARTICLE

Fracture Behavior of Nickel-Based Single Crystal Superalloy During High-Cycle Fatigue at 850 °C

Zhang Jingang[1,2], Liu Xinling[1,2], Chen Xing[1,2], Li Zhen[1,2], Liu Jiabin[1,2], Teng Peng[1,2], Liu Changkui[1,2]

[1] Failure Analysis Center of Aero Engine Corporation of China, AECC Beijing Institute of Aeronautical Materials, Beijing 100095, China; [2] Beijing Key Laboratory of Aeronautical Materials Testing and Evaluation, Beijing 100095, China

Abstract: The high-cycle fatigue fracture characteristics and damage mechanism of nickel-based single crystal superalloys at 850 °C was investigated. The results indicate that high-cycle fatigue cracks in single crystal superalloys generally originate from defect locations on the subsurface or interior of the specimen at 850 °C. Under the condition of stress ratio R=0.05, as the fatigue load decreases, the high-cycle fatigue life gradually increases. The high-cycle fatigue fracture is mainly characterized by octahedral slip mechanism. At high stress and low lifespan, the fracture exhibits single or multiple slip surface features. Some fractures originate along a vertical small plane and then propagate along the {111} slip surface. At low stress and high lifespan, the fracture surface tend to alternate and expand along multiple slip planes after originating from subsurface or internal sources, exhibiting characteristics of multiple slip planes. Through electron backscatter diffraction and transmission electron microscope analysis, there is obvious oxidation behavior on the surface of the high-cycle fatigue fracture, and the fracture section is composed of oxidation layer, distortion layer, and matrix layer from the outside to the inside. Among them, the main components of the oxidation layer are oxides of Ni and Co. The distortion layer is mainly distributed in the form of elongated or short rod-shaped oxides of Al, Ta, and W. The matrix layer is a single crystal layer. Crack initiation and propagation mechanism were obtained by systematical analysis of a large number of high-cycle fatigue fractures. In addition, the stress ratio of 0.05 is closer to the vibration mode of turbine blades during actual service, providing effective guidance for the study of failure and fracture mechanisms of turbine blades.

Key words: single crystal superalloys; high-cycle fatigue; oxidation behavior; slip; oxidation layer

1 Introduction

Nickel-based single crystal superalloys have been widely used as turbine blade materials in aircraft engines due to their exceptional creep resistance and thermal fatigue performance at elevated temperatures[1–3]. In practical applications, turbine blades must endure a variety of complex loads, including centrifugal forces, thermal stresses, and vibrational stresses. Consequently, the blade structure is susceptible to high-cycle fatigue failure under the combined influence of these multiple loading conditions[4]. Over the past few decades, high-cycle fatigue failure has emerged as one of the primary causes of turbine blade failures.

Researchers have conducted comprehensive studies on the high-cycle fatigue failure mechanisms in single crystal superalloys[5–12]. Their findings indicated that surface defects significantly diminish the high-cycle fatigue life of these materials, and all specimens with surface defects are found to contain multi-source fatigue cracks. Furthermore, it was observed that the fatigue life of single crystal superalloys decreases with an increasing stress ratio[13], with fracture modes transitioning from cleavage-like fractures at low stress ratios to dimple-like fractures at higher stress ratios. At low strain amplitudes, dislocations slip within the channels of the γ matrix. Conversely, at elevated strain amplitudes, dislocations shear through the γ' phase.

When further investigating the changes in dislocation structure during high-cycle fatigue, it was observed that in the

Received date: November 29, 2024
Foundation item: National Science and Technology Major Project (J2019-VI-0022-0138)
Corresponding author: Liu Xinling, Ph. D., Professor, Failure Analysis Center of Aero Engine Corporation of China, AECC Beijing Institute of Aeronautical Materials, Beijing 100095, P. R. China, E-mail: liuxinling119@163.com

early and middle stages of high-cycle fatigue testing, the primary deformation mechanism of single crystal superalloys is the movement of dislocations within the matrix. Two dislocations with distinct vectors converge on the same slip plane, resulting in a three-dimensional network structure[14]. In the final stage of high-cycle fatigue testing, this dislocation structure evolves to form persistent slip bands, which facilitate the reprecipitation of both γ and γ' phases. The interplay between cyclic plastic deformation and elevated temperatures leads to the formation of spherical and small secondary γ' phases within the matrix. This phenomenon impedes dislocation movement in the matrix and enhances fatigue strength.

When investigating the high circumferential bending fatigue performance of the third-generation single crystal superalloy DD9 at 800 °C, it was observed that under rotational bending loads, the surface of specimen experiences maximum cyclic stress. As the alloy undergoes slip and forms a slip band, phenomena such as intrusion and extrusion occur on the surface of specimen, making it susceptible to fatigue crack initiation in its weaker regions[15]. The deformation mechanism of single crystal superalloys is characterized by octahedral slip. Consequently, during fatigue crack propagation, the propagation plane aligns with the {111} plane. This behavior is consistent with typical high rotation bending fracture mechanisms, both exhibiting cleavage-like fracture characteristics.

According to a large number of failure cases, the blade is prone to cracking at the body part of a turbine blade, which is the first order bending vibration position. Simulation of the bend revealed that the actual service temperature at that position is 850 °C. At present, far fewer research reports on high-cycle fatigue of single crystal superalloys at 850 °C. In order to study the failure and fracture behavior of turbine blade during service, the fatigue test of the alloy was conducted at 850 °C. This study investigates the high-cycle fatigue fracture mechanism of single crystal superalloys at this temperature by conducting high-cycle fatigue tests on standard specimens, combined with the macroscopic and microscopic morphology of the fracture surface and the characteristics of microstructure evolution, providing support for the high-cycle fatigue failure behavior of single crystal turbine blades in practical engineering.

2 Experiment

The material used in the experiment was the second-generation nickel-based single crystal superalloy independently developed by China. The main components of these alloys are listed in Table 1. Single crystal superalloy specimens with [001] orientation were prepared using the spiral crystal selection method in a high-temperature gradient vacuum directional solidification furnace. The deviation between the crystal orientation measured using the X-ray backscattering method and the direction of the principal stress axis was within 15°. The test rod was processed into a high-cycle fatigue specimen after heat treatment. The microstructure after heat treatment and schematic diagram of standard specimen is shown in Fig.1.

The high-cycle fatigue test was conducted on a high-frequency fatigue testing machine using stress control. The experimental temperature was 850 °C, and the specimen was heated in a resistance furnace with a stress ratio of 0.05. The fatigue fracture surface was observed macroscopically and microscopically using Leca stereoscope and TESAN field emission scanning electron microscope (SEM). In order to study the microstructure evolution of the fracture section, Focused ion beam (FIB) was used to sample the fracture section on the fracture surface. Electron backscatter diffractometer (EBSD, Zeiss Gemini SEM300) was used to analyze the evolution of crystal orientation near the fracture, and transmission electron microscope (TEM, FEI Talos 200S) was used to analyze the microstructure evolution and element near the fracture.

3 Results and Discussion

3.1 High-cycle fatigue performance analysis

The relationship between the maximum loading stress σ_{max} and the fatigue life N_f under the condition of 850 °C and stress ratio of R=0.05 is shown in Fig. 2. When σ_{max} is between

Table 1 Chemical composition of nickel-based single crystal superalloys (wt%)

Cr	Co	W	Mo	Al	Ta	Re	Hf	Nb	Ti	Ni
4.8	9.5	9.0	2.5	6.2	8.5	2.4	0.15	1.2	0.1	Bal.

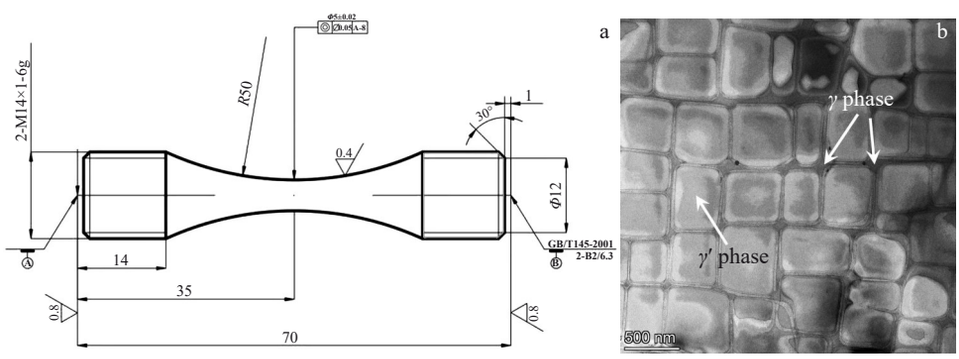

Fig.1 Schematic diagram of standard high-cycle fatigue specimen (a) and microstructure of nickel-based single crystal superalloy after heat treatment (b)

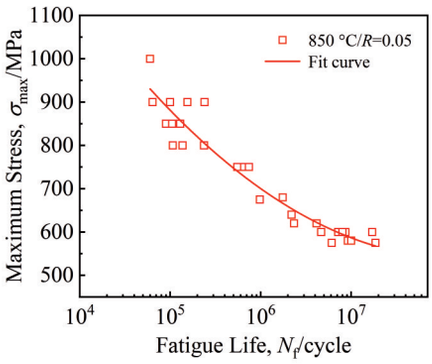

Fig.2 High-cycle fatigue performance of single crystal superalloy at 850 °C

800–1000 MPa, the high-cycle fatigue life of the single crystal alloy is approximately 10^5 cycles. As the applied load decreases, the high-cycle fatigue life gradually increases. When σ_{max} is 575 MPa, the high-cycle fatigue life of the alloy reaches around 10^7 cycles.

3.2 Analysis of macroscopic fracture

Generally, fatigue fractures can be divided into three stages: fatigue source zone, crack propagation zone, and transient fracture zone. For single crystal superalloys with [001] orientation, due to their face centered cubic structure, the slip system is prone to move along the {111} slip plane. The theoretical angle between the {111} slip plane and the axial direction is about 35.3° . In fact, during the alloy casting process, there is a slight deviation between the crystal growth direction and the [001] crystal direction, generally not exceeding 15° . Therefore, during the fatigue test, the angle between the inclined plane formed by the fatigue fracture and the axial direction is between 35–45°, and this inclined plane is the main slip plane of {111}.

Under the conditions of 850 °C and stress ratio R=0.05, the high-cycle fatigue fracture characteristics under different fatigue loads are shown in Fig.3, in which, the arrows indicate the direction of crack propagation. At this temperature, the fracture surface appears dark brown or dark blue. Owing to the octahedral slip mechanism, the fracture surface is mainly characterized by inclined surfaces, and there are differences in the fracture characteristics under different stress levels. At σ_{max} =850 MPa, the crack originates away from the surface of the specimen, and then propagates along three different directions of (111) slip planes. In the early stage of propagation, fatigue arc features are observed, and the extended edge features appear throughout the entire propagation process. Except for the rough slip step area at the junction of the two slip planes, the entire fracture surface is relatively flat, and no signs of compression wear are observed on the fracture surface. When σ_{max}=750 MPa, the fracture surface exhibits a single inclined surface feature, and the crack originates along the subsurface. The fatigue arc feature can be observed during the stable propagation stage. When σ_{max} =580/620 MPa, the number of slip planes on the fracture surface increases. After originating along the subsurface or interior, the crack propagates along a

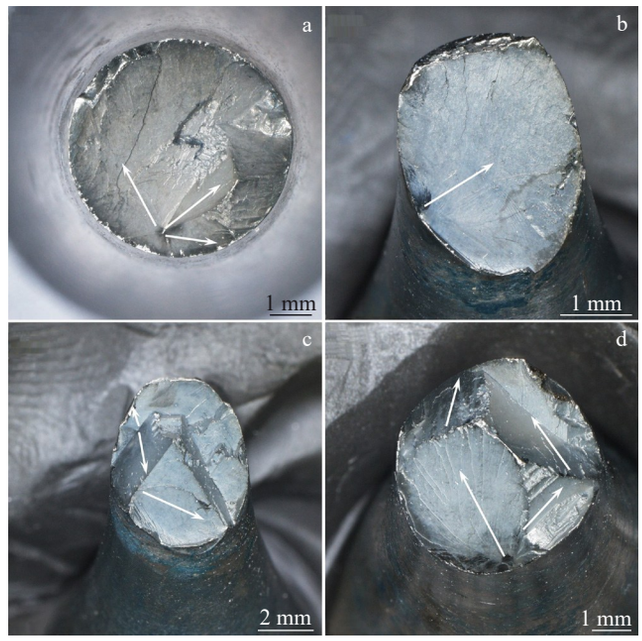

Fig.3 High-cycle fatigue fracture characteristics at 850 ° C and R= 0.05 under different loads: (a) σ_{max}=850 MPa, (b) σ_{max}=750 MPa, (c) σ_{max}=620 MPa, and (d) σ_{max}=580 MPa

single or multiple slip planes. During the propagation process, the crack alternates along different slip systems, resulting in the fracture surface exhibiting multiple inclined features.

3.3 Analysis of crack initiation and propagation

By observing the high-cycle fatigue fracture, the characteristics of fracture can be divided into three types: single slip surface features, small plane multiple slip surface features on a vertical axis, and multiple slip surface features. Between 750 –900 MPa, the fatigue life of the specimen is less than 10^6 cycles, and the fatigue fracture surface contains the three typical fracture characteristics mentioned above. When σ_{max}<680 MPa and the fatigue life is higher than 10^6 cycles, the fracture characteristics are mainly characterized by multiple slip surfaces.

Under high stress conditions, the three typical fracture characteristics of high-cycle fatigue fractures are mainly characterized by a single vertical axial small plane and multiple slip surfaces. As shown in Fig. 4, the high-cycle fatigue life at 900 MPa is 10^5 cycles, which belongs to the low lifespan fracture in the high-cycle fatigue category. From Fig. 4b, it can be seen that the crack originates along the casting defect inside the specimen, and there is a small cubic plane perpendicular to the axial force near the casting defect. When the crack propagates on the cubic small plane, it leaves a fan-shaped fatigue zone expansion mark.

Analysis of the crack propagation path reveals that the crack begins to propagate along the (001) slip plane and two different (111) slip planes after initiation along the defect. When the propagation path on the (111) slip plane is obstructed, the crack continues to propagate along the {111} slip plane through the cross-slip mechanism. Fig.4c shows the fatigue band characteristics of crack propagation on the (111)

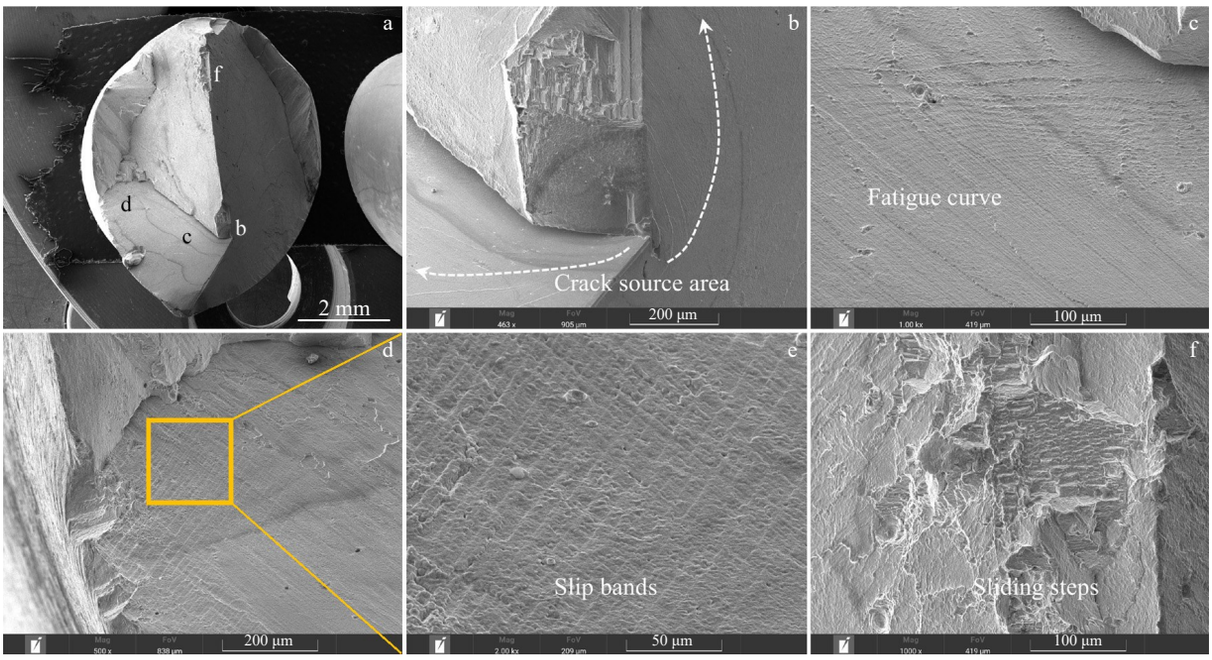

Fig.4 Fracture characteristics at different stages of crack propagation under condition of 900 MPa: (a) macroscopic fracture morphology, (b) small planes in crack source area, (c) stable propagation zone, (d–e) rapid propagation zone, and (f) boundary between two slip surfaces (Fig.4b, 4c, 4d, and 4f correspond to regions b, c, d, and f marked in Fig.4a, respectively)

slip plane, with the fatigue bands showing a trend from dense to sparse along the direction of crack propagation. Fig. 4d shows the surface slip band morphology during the rapid crack propagation stage. Generally, when the single slip plane rapidly expands, the fracture surface of single crystal superalloys exhibits an extended edge morphology. When the crack propagates to the later stage or is about to undergo a change in the slip plane, the fracture surface exhibits the parallel slip band characteristics shown in Fig. 4d – 4e. Zooming into the local area reveals that the slip bands are parallel to each other and perpendicular to the direction of the extended edge lines. Fig.4f shows the slip step characteristics formed at the junction of two {111} slip planes in the later stage of crack propagation. This morphology is a characteristic of the rapid tearing between two sections under high stress during the final stage of crack propagation. The sliding step exhibits a clear morphology, and no signs of wear or compression are observed.

Fig. 5 shows the typical characteristics of single sliding surface of high-cycle fatigue fracture under high stress conditions. The load of the specimen is 750 MPa, and the fatigue life is 7.42×10^5 cycles. As shown in Fig.5b, the crack originates from the subsurface casting defects of the specimen. Under microscopic conditions, it can be observed that the crack after origination propagates along two different (111) slip planes, and the secondary slip planes can be ignored owing to their small proportion. The fracture surface during the stable expansion stage exhibits characteristics of fatigue arc at the macroscopic level. The observation of partially peeled fracture surfaces reveals the presence of a distinct oxidation layer on the fracture surface at 850 °C. The surface of the oxidation layer is distributed in a spinel shape and has good density. The specimen matrix is composed of γ channels and γ' phase structure, and the matrix structure is similar to a triangular γ' phase composition. It can be determined that the crystal plane, where the fracture is located, is the {111} slip plane.

Fig. 5d shows the fracture morphology near the extended edge line of the rapid expansion zone. It can be seen that there are a large number of parallel strip-shaped slip bands near the extended edge line. Unlike Fig.5e, this slip band is consistent with the direction of the extended edge line. Fig.5e shows the evolution of crack propagation edge lines into cross-slip propagation surface in the later stage of crack propagation. The slip bands within the propagation edge lines are consistent with those in Fig. 5d. When the crack propagates to the final stage on the single slip plane and rapid fracture is about to occur along other crystal planes, the fracture morphology is shown in Fig.5f. There is a rough slip step zone at the junction of the two slip surfaces, and the morphology of the layered slip step is almost perpendicular to the direction of crack propagation.

From the above analysis, it can be inferred that when the fracture exhibits the single sliding surface feature, the {111} sliding surface has a low propagation resistance, and the crack propagates alternately along countless parallel slip bands under shear stress, which are aligned with the direction of the extended edge lines. When cracks propagate alternately along multiple slip planes, crack propagation is hindered in the later stage of single slip plane propagation, resulting in parallel slip

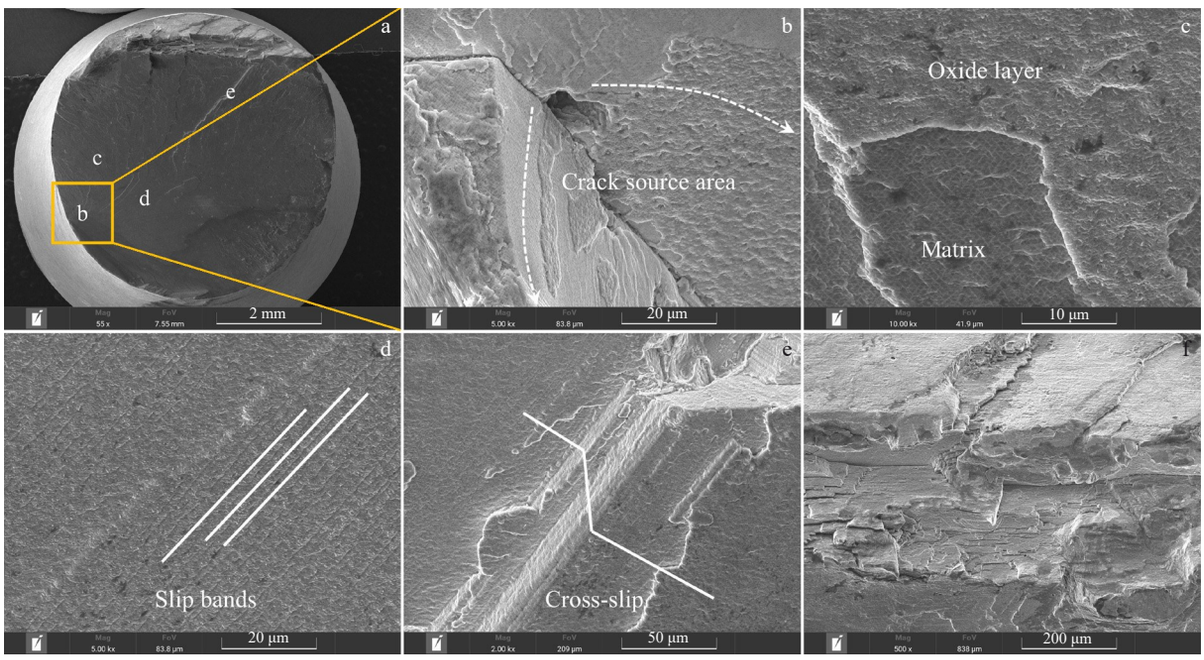

Fig.5 Typical characteristics of high-cycle fatigue fracture under condition of 750 MPa: (a) macroscopic fracture morphology, (b) crack source area, (c–e) crack propagation stage, and (f) slip step (Fig.6c–6e correspond to regions c–d marked in Fig.5a, respectively)

bands perpendicular to the propagation direction. The boundary position of the slip planes tends to produce slip steps perpendicular to the crack propagation direction.

When the load is reduced to 580 MPa, the fatigue life of the alloy approaches the fatigue limit. As shown in Fig. 6, compared with the fracture of low lifespan, there are multiple slip surfaces on the fracture surface under this condition. In Fig. 6a, the crack originates along the subsurface, and no casting defects are found at the origin location. The crack source area exhibits a fan-shaped pit characteristic. After the crack initiates, it propagates along the {111} slip plane, and fatigue band characteristics appear on the cross-section approximately 2 mm away from the crack source area. After the current slip plane propagation is blocked, the crack continues to propagate along the other three {111} slip planes in different directions. As shown in Fig. 6c, the crack originates along the irregular casting defect and simultaneously propagates along multiple {111} slip planes, exhibiting fatigue band characteristics at a distance of more than 1 mm from the crack source area. By observing the characteristics near the casting defects in the crack source area, it is found that there are multiple convex deformation features along the periphery of the defects, and the cracks propagate in different directions along these features.

In summary, under the condition of 850 °C and R=0.05, the fracture mode of high-cycle fatigue is mainly characterized by octahedral slip mechanism. At high stress and low lifespan of the specimen, the fracture surface exhibits single or multiple slip surfaces features, and some fractures originate along a vertical small plane and then propagate along the {111} slip surface. At low stress and high fatigue lifespan, the fracture surface is prone to alternate and expand along multiple slip

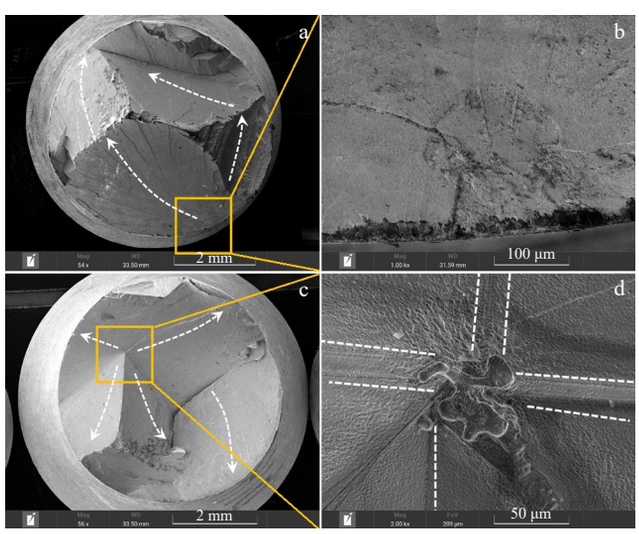

Fig.6 Typical characteristics of high-cycle fatigue fracture under condition of 580 MPa: (a–b) subsurface source; (c–d) internal source

planes after originating from subsurface or internal sources, exhibiting characteristics of multiple slip planes.

In order to study the changes in the longitudinal section structure near the fracture surface, the longitudinal section of the high-cycle fatigue fracture was sampled from the crack source area according to the main crack propagation direction. The macroscopic characteristics are shown in Fig. 7a, and the crystal plane of the longitudinal section is (011). The left side in Fig. 7a is the crack source area, and the crack propagates from the bottom left to the top right direction.

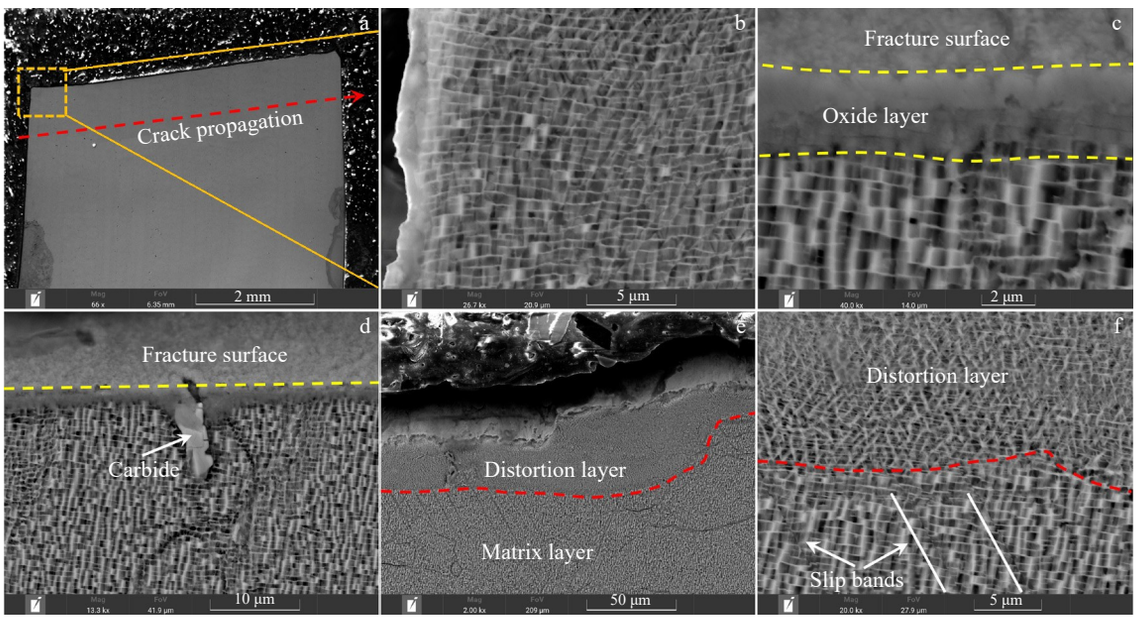

Fig.7 Structural characteristics of longitudinal section of high-cycle fatigue fracture along the crack growth direction under condition of 750 MPa: (a) macromorphology; (b) fatigue source area; (c–d) stable extension zone; (e–f) wear and deformation in rapid expansion zone

As shown in Fig. 7b, there is slight deformation of the matrix structure along the crack propagation direction near the outer surface of the specimen. After corrosion, a thin oxidation layer is present on the outer surface of the specimen. The stable expansion zone on the fracture surface has a dense oxidation layer with a thickness of about 3.3 μm, and no abnormalities are observed in the underlying matrix structure. From the analysis of morphological features, it can be seen that the oxidation layer on the fracture surface is a layered structure, including an outer oxidation layer and an inner oxidation layer. In addition, as shown in Fig.7d, carbide exists between dendrites near the section along the crack growth direction, and oxidation penetrates deep into the matrix along the carbide location.

During the rapid crack propagation stage, wear and extrusion characteristics can be seen in the local area, as shown in Fig.7e. The extrusion depth is 30–50 μm, which is obviously different from the morphology of the matrix. Local observation at high magnification shows that the microstructure in the extrusion zone has obvious plastic deformation, and the matrix structure is a cubic frame structure. After extrusion deformation, the microstructure in the extrusion zone is a triangular structure, which is similar to the crystal plane structure of (111). Moreover, there are a large number of parallel slip lines in the matrix below the deformation layer, as shown by the white line segment in Fig.7f.

According to the above analysis, in the early stage of crack growth and the stable growth stage of high-cycle fatigue, the structural characteristics of the fracture section are single, and the microstructure near the fracture has no obvious deformation characteristics except for the oxidation layer. During the rapid propagation stage, the fracture surface has wear and extrusion characteristics, the direction of the microstructure changes after deformation in the deformation layer, and there are a lot of tilt and slip characteristics in the matrix.

3.4 Plastic deformation analysis of fracture surface

EBSD can help analyze the crystal structure, crystal orientation, and other related information of materials. Although single crystal superalloys do not have grain boundaries, their matrix structure is composed of γ channels and cubic γ' phases. During fatigue testing, the matrix near the crack tip is prone to plastic deformation under alternating loads. EBSD can more intuitively express the plastic deformation of the fracture surface through the orientation changes of the microstructure.

Through analysis of the high-cycle fatigue fracture at 850 °C, it is found that there is a significant oxidation layer on the surface of the fracture, and the oxidation layer exhibits delamination. Due to the thin oxidation layer thickness, SEM can only make preliminary judgments of the oxidation layer, and more microscopic and detailed morphology cannot be obtained. In order to further investigate the surface oxidation behavior of high-cycle fatigue fracture under the condition of 850 °C/R=0.05, FIB specimens were taken from the fatigue fracture under microscopic conditions. After sampling, the oxidation mechanism of the fracture surface was obtained by EBSD and TEM analysis.

For high-cycle fatigue fracture, there are three stages of fatigue crack propagation: initiation, stable propagation, and fast propagation. Due to the ongoing application of alternating fatigue loads, there is a sizable plastic zone in the stress concentration zone during the crack initiation stage, even before the fracture occurs. The majority of high-cycle fatigue fractures are caused by casting defects. Consequently, the plastic zone and oxidation situation during the initiation stage

can be characterized by sampling vertical section of the fracture surface close to the defect.

The crack firstly appears at the casting defect within the specimen, which is situated on the {111} slip plane, as seen in Fig. 8a. As indicated in Fig. 8b, FIB specimens were taken along the vertical fracture path close to the casting defect, whose cross-sectional dimension is 5 μm×5 μm.

The fracture section near the fatigue source area was subjected to EBSD analysis, and the resulting inverse pole figure (IPF) along *Z*-axis is shown in Fig. 8c. On the fracture surface, a layer of grain with clear boundaries is formed, and the distinction in crystal orientation between neighboring grains can be identified by comparing the colors of the grains. Beneath the oxidation layer is a transition layer, most of the areas within which are unable to recognize crystallographic information based on element Ni. This region is also referred to as a distortion layer. Below the transition layer is the Ni matrix, and the crystallographic information recognition of element Ni in the matrix layer is relatively high. The Ni matrix approaches the (001) crystal plane in the *Z*-axis direction of IPF. According to the orientation difference analysis of the Ni matrix layer, as displayed in Fig. 8f, the matrix still exhibits single crystal properties because the overall orientation difference is less than 10°. Fig. 8g displays the misorientation angle distribution of the oxidized grains on the fracture surface. The outermost oxidation layer of the fracture has a polycrystalline structure because the orientation difference is dispersed over the range of 0°–60° and can reach up to 60° between random grains. Fig. 8d shows the kernel average misorientation (KAM) map of the fracture section. It can be seen that only some of the grains in the surface oxidation layer have deformation characteristics, and plastic deformation is mainly concentrated in the transition layer. The plastic deformation parameters along the fracture surface towards the interior of the matrix were measured, as shown in Fig. 8e, and there is significant plastic deformation at a distance of 1.4 μm from the surface.

3.5 TEM analysis of fatigue fracture

During the TEM analysis process, energy dispersive X-ray spectroscope (EDS) was used on the fracture section of the fatigue source area, and the results are shown in Fig. 9. The outermost oxidation layer is mainly composed of elements Ni, Co, and O, while the short rod-shaped structure in the distortion layer is mainly composed of elements Al and O. Elements Ni and Al are mainly distributed in the cubic γ' phase of the matrix, while Co, Cr, Re and other elements are distributed in the γ channels as strengthening elements for the matrix.

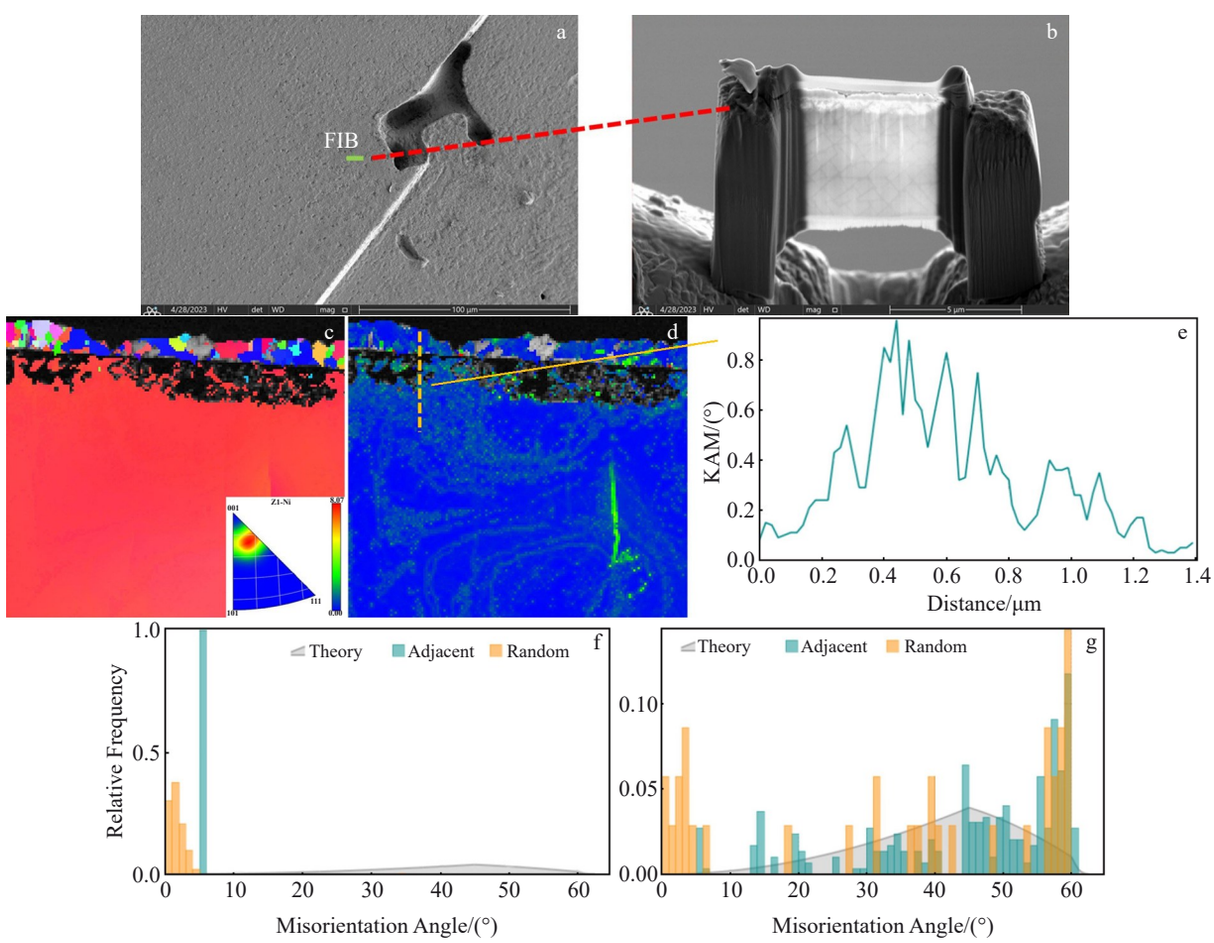

Fig. 8 EBSD analysis results of crack source area of high-cycle fatigue fracture with σ_{max}=640 MPa and N_f=2.195×10^6 cycles: (a) FIB sampling location, (b) morphology of FIB, (c) IPF along *Z*-axis, (d) KAM map, (e) distribution of KAM along the line marked in Fig. 8d, (f) misorientation angle distribution of Ni matrix layer, and (g) misorientation angle distribution of oxidized grains

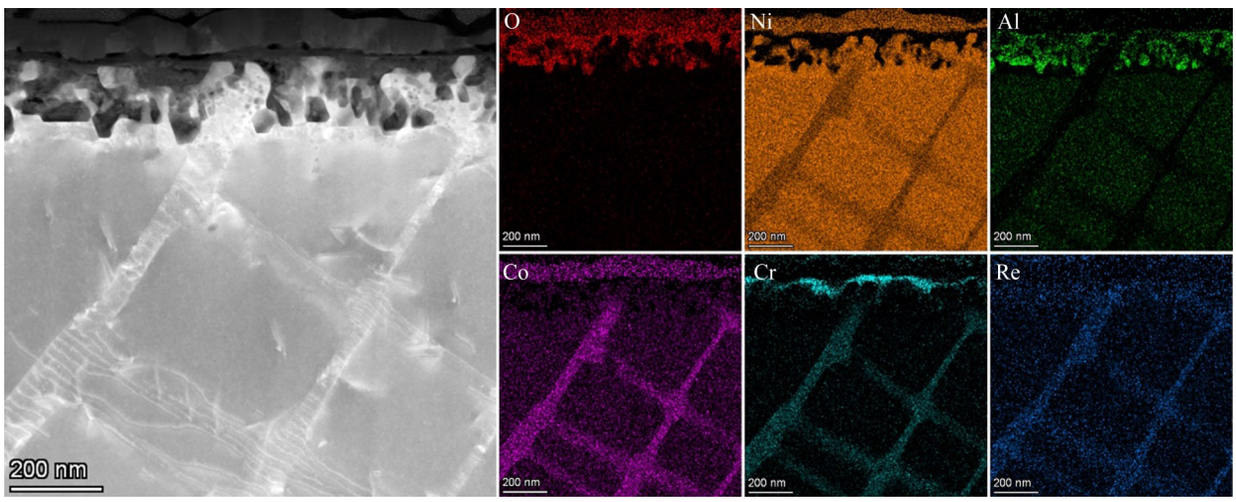

Fig.9 TEM image and corresponding EDS element mappings of fracture section near the fatigue source area

Local element content analysis was conducted on six different points within the oxidation layer and distortion layer on the fracture surface. The analysis points are shown in Fig. 10, with large grains, medium grains, small grains, and distortion layer at different depths from the surface inward. The large grains in the outer layer of the oxidation layer and the grains in the inner layer are mainly composed of elements O, Co, Ni, as well as a small amount of elements Ta and W. The outermost layer has a slightly higher Co content. For small grains at the boundary between the oxidation layer and the distortion layer, the content of elements Co and Ni decreases significantly compared to the outer grains, while the content of elements Ta and W increases, and the content of element Al slightly increases. The content of elements Al, Cr, Ta, and W in the distortion layer is significantly increased, while the content of elements Ni and Co is decreased. The specific element content of

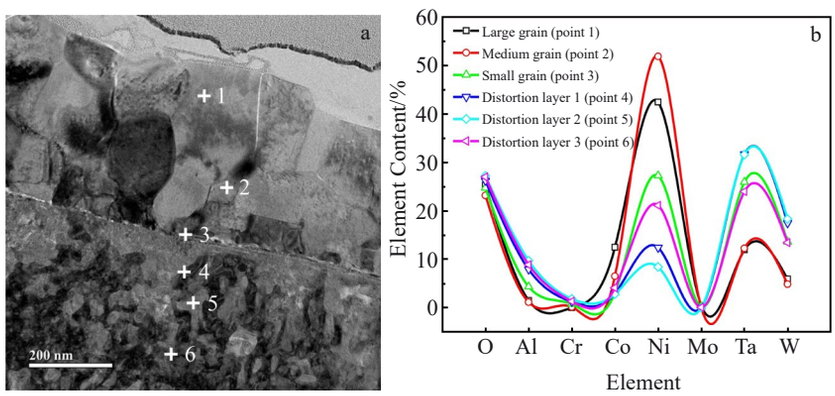

Fig.10 TEM image of oxidation layer and distortion layer on fracture surface (a) and variation curves of element content at different points marked in Fig.10a (b)

each part is shown in Table 2.

According to analysis, during the fatigue fracture oxidation process at 850 °C, elements Ni and Co migrate to the surface and are preferentially oxidized into grain morphology attached to the outermost surface of the fracture. The migration speed of elements Al, Cr, Ta, and W to the surface is slow, so the outer grains only contain trace amounts of elements Al, Cr, Ta, and W, which are mainly distributed in the distortion layer. Due to the precipitation of elements Ni and Co in the distortion layer, the Ni_3Al structure is destroyed, and the morphology of the original γ channel and cubic γ' phase disappears. Due to the temperature field, elements Al, Ta, and

Table 2 Element content at different points marked in Fig. 10a (wt%)

Point	O	Al	Cr	Co	Ni	Mo	Ta	W
1	25.32	1.50	0	12.47	42.43	0.43	11.96	5.90
2	23.19	1.14	0.17	6.53	51.87	0	12.26	4.85
3	24.75	4.35	0.78	3.14	27.26	0.20	25.94	13.59
4	26.21	7.91	1.23	2.96	12.40	0.11	31.70	17.48
5	27.23	9.74	1.84	2.82	8.42	0	31.62	18.33
6	27.00	8.88	1.34	4.12	21.13	0.09	24.00	13.44

W in the cubic γ' phase are distributed in the distortion layer in the form of long or short rod-shaped oxides. Due to the continuous effect of temperature field, the oxidation behavior continues to intensify, and the elements Ni and Co inside the matrix also migrate to the outer surface. When elements Ni and Co pass through the distortion layer, they are oxidized inside the distortion layer and distributed in the form of oxidized grains.

4 Conclusions

1) Under the condition of 850 °C and stress ratio R=0.05, as the fatigue load decreases, the high-cycle fatigue life gradually increases. Under this condition, the fatigue limit of single crystal superalloy is about 575 MPa.

2) Under the condition of 850 °C and stress ratio R=0.05, the high-cycle fatigue fracture is mainly characterized by octahedral slip mechanism. At high stress and low lifespan, the fracture exhibits single or multiple slip surfaces features, and some fractures originate along a vertical small plane and then propagate along the {111} slip surface. At low stress and high lifespan, the fracture surface tends to alternate and propagate along multiple slip planes after originating from subsurface or internal sources, exhibiting characteristics of multiple slip planes.

3) Under the condition of 850 °C and stress ratio R=0.05, the high-cycle fatigue fracture section consists of a oxidation layer, a distortion layer, and a matrix layer from the outside to the inside. Among them, the oxidation layer consists of large grains, medium grains, and small grains from the surface to the inside, mainly composed of Ni and Co oxides. The elements Al, Ta, and W are distributed in the distortion layer in the form of long or short rod-shaped oxides. The matrix layer is a single crystal layer with an overall orientation difference within 10°.

References

1 Pollock T M, Sammy T. *Journal of Propulsion and Power*[J], 2006, 22(2): 361

2 Cervellon A, Hémery S, Kürnsteiner P *et al*. *Acta Materialia*[J], 2020, 188: 131

3 Reed R C, Cox D C, Rae C M F. *Materials Science and Engineering A*[J], 2007, 448(1–2): 88

4 Cervellon A, Cormier J, Mauget F *et al*. *Metallurgical and Materials Transactions A*[J], 2018, 49: 3938

5 Shi Z X, Zhao J Q, Liu S Z *et al*. *Nonferrous Metals Science and Engineering*[J], 2018, 9(6): 5

6 Han M, Xie H J, Li J R *et al*. *Journal of Materials Engineering*[J], 2019, 47(6): 8

7 Hu C Y, Liu X L, Tao C H *et al*. *Journal of Materials Engineering*[J], 2017, 45(4): 84

8 Shui L, Jin T, Sun X F *et al*. *International Journal of Modern Physics B*[J], 2010, 24(16): 2886

9 Yu J J, Yang Y, Sun X F *et al*. *Journal of Materials Science*[J], 2012, 47(12): 4805

10 Yu J J, Sun Y L, Sun X F *et al*. *Materials Science and Engineering A*[J], 2013, 566: 90

11 Zhang J G, Chen X, Li Z *et al*. *Rare Metal Materials and Engineering*[J], 2023, 52(6): 1985

12 Zhang J G, Liu X L, Chen X *et al*. *Rare Metal Materials and Engineering*[J], 2024, 53(9): 2458

13 Xie Hongji, Li Jiarong, Han Mei *et al*. *Rare Metal Materials and Engineering*[J], 2018, 47(11): 3381

14 Shui L, Xu Y C, Hu Z Q. *Rare Metal Materials and Engineering*[J], 2018, 47(4): 1054

15 Shi Z X, Wang X G, Liu S Z. *Materials and Mechanical Engineering*[J], 2016, 40(1): 5

镍基单晶高温合金850 ℃高周疲劳断裂行为

张金刚[1,2]，刘新灵[1,2]，陈　星[1,2]，李　振[1,2]，刘佳宾[1,2]，滕　鹏[1,2]，刘昌奎[1,2]

(1. 中国航发北京航空材料研究院 中国航发失效分析中心，北京 100095)

(2. 航空材料检测与评价北京市重点实验室，北京 100095)

摘　要：对镍基单晶高温合金在850 ℃的高周疲劳断口特征及损伤机制进行研究。结果表明：在850 ℃时单晶高温合金高周疲劳裂纹一般萌生于试样亚表面或内部的缺陷位置。在应力比R=0.05的条件下，随疲劳载荷降低，高周疲劳寿命逐渐增加。高周疲劳断口主要以八面体滑移机制为主，在大应力低寿命时断口呈单个或多个滑移面特征，部分断口沿垂直小平面起源后再沿{111}滑移面扩展；在低应力高寿命时，断口沿亚表面或内部起源后易沿多个滑移面交替扩展，断口呈多个滑移面特征。通过电子背散射衍射分析和透射电镜分析可知，高周疲劳断口表面存在氧化行为，断口截面由外往内依次为氧化层、畸变层和基体层。其中，氧化层主要成分为Ni、Co氧化物；畸变层内主要为长条状或短棒状的Al、Ta、W氧化物形貌分布；基体层为单晶层。本研究对大量高周疲劳断口进行系统分析得到其裂纹萌生及扩展规律，应力比为0.05更接近涡轮叶片实际服役过程中的振动模态，为涡轮叶片的失效断裂机制奠定了基础。

关键词：单晶高温合金；高周疲劳；氧化行为；滑移；氧化层

作者简介：张金刚，男，1995年生，博士，中国航发北京航空材料研究院中国航发失效分析中心，北京 100095，E-mail：jingangpri@163.com